

Crystallization of amorphous superlattices in the limit of ultrathin films with oxide interfaces

M. Zacharias^{1,*} and P. Streitenberger²

¹*Institute of Experimental Physics, Department of Solid State Physics, Otto-von-Guericke-University Magdeburg, Germany*

²*Institute of Experimental Physics, Department of Materials Physics, Otto-von-Guericke-University Magdeburg, Germany*

(Received 10 March 2000)

Annealing of amorphous Si/SiO₂ or Ge/SiO₂ multilayers produces nanocrystals embedded between oxide interfaces. It is found that the crystallization temperature is strongly enhanced by the presence of the oxide interfaces and follows an exponential law. The crystallization temperature increases rapidly with decreasing Si layer thickness, and a nonstoichiometric interface decreases the crystallization temperature compared to a stoichiometric interface of the same thickness. A model is presented that takes into account the interface energies, the thickness of the layer, the melting point of the system, and the crystallization temperature of the thick amorphous layer. The evidence for a critical crystallization radius and the influence of deviations from a perfect stoichiometric interface are discussed.

INTRODUCTION

Polycrystalline thin films are essential for modern electric, optic, and magnetic devices such as Si-based thin-film transistors, solar energy converters, or magnetic recording media, and have been used in Si integrated-circuit technology since the 1970s. Today, polycrystalline Si is applied in ultralarge-scale integration technology for both active and passive components. For device application precise engineering of the Si grain size with focus on control in grain boundary and defect density is essential.

The solid-phase crystallization of chemical-vapor-deposited amorphous Si films of thickness above 50 nm has been reviewed extensively.¹ However, there are only a few data at hand for the crystallization behavior at thickness below 50 nm. The existing models for the kinetical mechanisms of crystal grain growth are not applicable in the presence of a second SiO₂ top oxide layer or multiple stacks of Si/SiO₂ periods. The nucleation of nanocrystals in ultrathin layers capped with thin oxide layers has not been as extensively studied yet as epitaxial growth. There are only a few reports related to nanocrystal growth in ultrathin films with an oxide interface on both sides of the thin Si layer.²⁻⁴ In contrast to solid bulk phase crystallization and in the absence of a preexisting crystalline-amorphous interface, the amorphous-to-crystalline phase transition occurs through random nucleation of crystalline clusters surrounded by amorphous material under the strain field of the superlattice structure. Compared to solid bulk phase crystallization the process involves several additional phenomena such as the creation of the crystalline seeds themselves, the influence of the oxide interface, the influence of strain, the influence of extended defects at the grain surface, etc. Also, it has been reported that nucleation of Si near the SiO₂ interface is prevented in the first adjacent 0.5–1.0 nm of the Si layer.⁵

An increase of the crystallization temperature by around 300 K is reported for amorphous Si/SiO₂ superlattices when the Si layer thickness is reduced to 2 nm.⁶ Lu, Lockwood, and Baribeau⁷ reported that ultrathin epitaxial Si/SiO₂ superlattices (2.8 nm) do not crystallize even at 1100 °C, which is around 300 K above the reported crystallization temperature

of a thick amorphous Si film (700 °C). A similar behavior is demonstrated for *a*-Ge/SiO₂ multilayers, where the crystallization temperature significantly increases. The crystallization temperature of thick amorphous Ge is reported to be 500 °C. However, a 1.7 nm amorphous Ge layer did not show crystallization even after annealing at 760 °C.³ Also, it has been found that the crystallization temperature of amorphous Si/Si₃N₄:H superlattices strongly depends on the *a*-Si:H well layer width. No crystallization appears for annealing at 800 °C using a layer thickness below 5 nm.⁸ Such a behavior is different, e.g., from that of a Si/Ge superlattice, which shows interdiffusion at the interface boundaries upon annealing that is easily detectable by Raman spectroscopy.⁹ The aim of this paper is to study the general character of the crystallization behavior as a function of reduced layer thickness. A model is developed to reveal the origin of such a strong and systematic increase in crystallization temperature with decreasing layer thickness.

EXPERIMENTAL DETAILS

Amorphous Si/SiO₂ multilayers are prepared using rf sputtering and plasma oxidation. The thickness of the amorphous Si layer is varied from 1.9 to 20 nm while the thickness of the amorphous SiO₂ layer is held constant (~3 nm). All samples are prepared on Si wafers to allow high-temperature annealing. Conventional furnace annealing is used for crystallization in the temperature range of 700–1050 °C. Every sample is annealed once. The temperature is raised by 50 K from sample to sample, which results in a determination error for the occurrence of crystallization of around 25 K. The crystallization state is investigated by wide-angle x-ray scattering,¹⁰ transmission electron microscopy (TEM), and high-resolution TEM. The state of crystallization is evidenced by the splitting of the (220) and (311) Bragg peaks in wide-angle x-ray scattering. Crystal size and inhomogeneous strain have different angle-dependent influences on the Bragg diffraction lines. Thus size and strain can be separated by a careful two-line Scherrer analysis as described in Ref. 10.

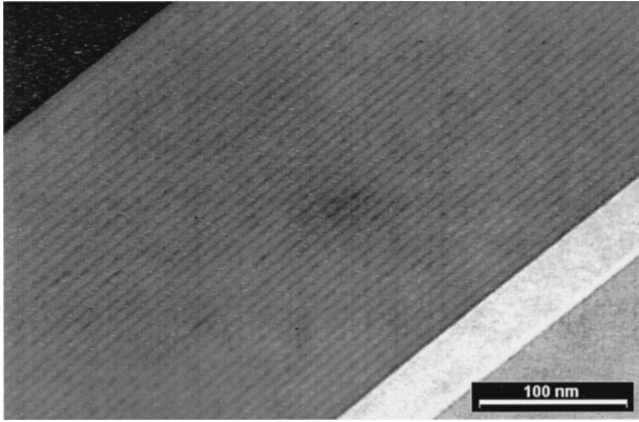


FIG. 1. TEM image of a Si/SiO₂ superlattice structure after crystallization.

RESULTS

Figure 1 shows the transmission electron image of a crystallized superlattice sample. The brighter and darker layers are the *a*-SiO₂ and the nc-Si layers, respectively. No disturbance of the superlattice structure can be seen due to the high-temperature annealing even for ultrathin layers. The roughness of the interface is less than 1 nm estimated from x-ray reflectivity.⁶ Figure 2 shows the crystallization temperature of an ensemble of superlattices based on different materials and interfaces as a function of the layer thickness, where the crystallization behavior of Si/SiO₂,⁴ Si/SiO_x,² and³ Ge/SiO₂ have been considered. Similar behavior is reported for Ge:H/GeN_x superlattices.¹¹ We found an increase in crystallization temperature by 300 K for a Si/SiO₂ superlattice with a 3 nm SiO₂ layer. As can be seen in Fig. 2 the crystallization temperature increases exponentially with decreasing layer thickness in all these different systems. Em-

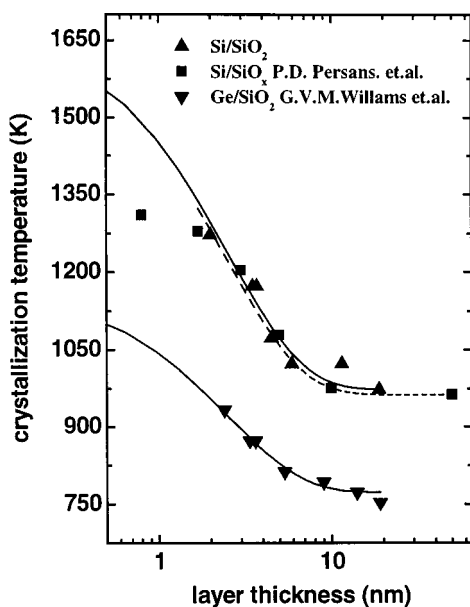


FIG. 2. Crystallization temperatures of different superlattice structures as a function of the layer thickness. The lines represent the model calculations using Eq. (1) and the parameters given in Table I.

TABLE I. Parameters used in Eq. (1) for fitting the data in Fig. 2.

Superlattice material	T_{melt} (K)	T_{ac} (K)	C (nm)
Si/SiO ₂	1683	973	2.56
Ge/SiO ₂	1211	773	2.52

pirically, this exponential increase of the crystallization temperature can be fitted by

$$T_c = T_{ac} + (T_{\text{melt}} - T_{ac})e^{-d/C}, \quad (1)$$

where T_{melt} represents the melting temperature of bulk crystalline material, T_{ac} is the crystallization temperature of a thick bulk amorphous film, and d is the real thickness of the layer. Thus the experimental data for the superlattice sets presented in Fig. 2 are fitted using the values summarized in Table I.

In addition, the inhomogeneous strain of Si/SiO₂ films is investigated as a function of the Si layer thickness d at the crystallization temperature T_c (Fig. 3). It is found that the inhomogeneous strain increases exponentially with decreasing layer thickness. The solid line in Fig. 3 represents a fit of the data using an exponential dependence on the Si layer thickness $\sim \exp(-d/2.56)$ (d in nm). Thus, strain and crystallization temperature follow a similar dependence on the Si layer thickness independent of the material sandwiched between the oxide interfaces.

CRYSTALLIZATION MODEL

A crystalline cluster nucleates homogeneously within the amorphous film or heterogeneously on discontinuities such as precipitates, defects, interfaces, etc. In the case of thick amorphous films the kinetics of the amorphous-to-polycrystalline phase transition is described by classical nucleation theory,¹ which is based on capillary effects at the crystalline-amorphous interface. However, an amorphous SiO₂ interface on both sides of a thin Si layer (less than 50

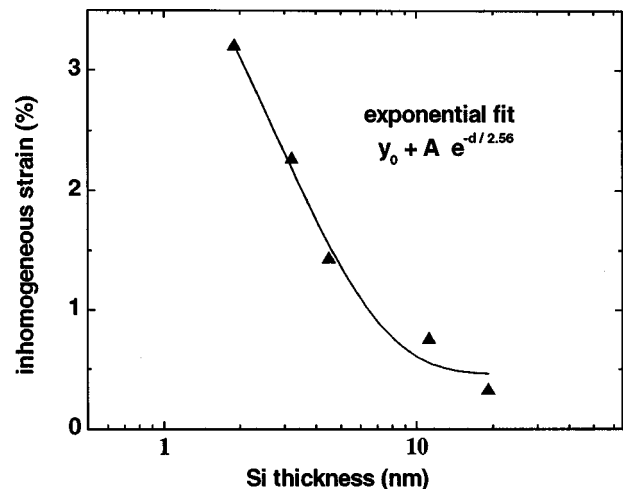


FIG. 3. Inhomogeneous strain as a function of the layer thickness.

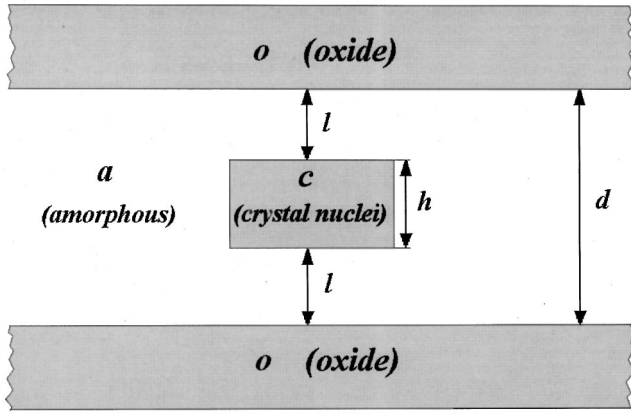


FIG. 4. Model of a cylindrically shaped nanocrystal embedded in an amorphous film with oxide interfaces.

nm) will not result in a homogeneous and uninfluenced nucleation within the layers.

As in Refs. 2 and 11, we assume here that the crystallization nucleus is symmetrically embedded in the amorphous material between the oxide interfaces and is cylindrical in shape. However, we introduce an additional spacing l which corresponds to a finite separation of the nucleus from the boundaries represented by the material o . In Fig. 4, the material o is the amorphous oxide phase, material a the amorphous semiconductor phase, and material c the crystallized semiconductor phase. In principle, for each combination of phases we assume that a well-defined, i.e., sharp and perfect, interface bounded by bulk material can be formed, which is characterized by its specific free interface energy. Accordingly, we define γ_{ac} , γ_{oc} , and γ_{oa} as the interfacial free energies per unit area between the amorphous (a) and crystalline (c) semiconductor phases (a/c), between the oxide material o and the crystalline (c) semiconductor phase (o/c), and between the oxide material o and the amorphous (a) phase (o/a), respectively. However, for the sandwich structure considered in Fig. 4, the interfaces between materials o and c are not well defined if the distance l between these materials is of the order of magnitude of only a few lattice constants, which is the case when the layer thickness is very small. For $l=0$, that is, $h=d$, we can assume that a sharp interface with the specific interface energy γ_{oc} is formed. In the other limit, for l very large ($l \rightarrow \infty$), the materials o and c are separated by two noninteracting, i.e., well-defined, perfect interfaces, namely, the interface between the materials c and a and the interface between the materials a and o . In order to rationalize the interaction between these two interfaces for small l , an effective interface energy is defined, which interpolates between the above well-defined limiting cases. In other words, we adopt the concept of an effective interface layer or a quasi-interface for interface phase transitions (see, e.g., Ref. 12) and assume that a quasiamorphous layer (the so-called quasi-interface) is formed in the space between materials o and c , which may be the result of the interatomic interaction between the two materials at small separation l . The effective free interface energy γ_{oc}^{eff} of this quasi-interface will be between that of a true amorphous/crystalline interface γ_{ac} and the specific free energy γ_{oc} of a true oxide/crystalline interface. Hence, we write

$$\gamma_{oc}^{\text{eff}} = \gamma_{ac} + (\gamma_{oc} - \gamma_{ac})M, \quad (2)$$

with M is an effective order parameter which is normalized to unity for the true oxide/crystalline interface and zero for the true amorphous/crystalline interface. In view of the measured inhomogeneous strain of the superlattice system as a function of the layer thickness (Fig. 3), M is expected to be an exponentially decreasing function of the interface spacing l ,

$$M = e^{-l/l_0}, \quad (3)$$

resulting for Eq. (2) in adjacent oxide/crystal materials with $\gamma_{oc}^{\text{eff}} = \gamma_{oc}$ for $l \rightarrow 0$, or adjacent amorphous/crystalline materials with $\gamma_{oc}^{\text{eff}} = \gamma_{ac}$ for $l \rightarrow \infty$. Assuming short-range interatomic forces, l_0 can be interpreted as an average screening or bonding length which is related to the range of interatomic forces typical for the materials o and c .

Using the above assumptions the Gibbs free energy for the cylindrically shaped nucleus with radius r (crystalline phase c) in Fig. 4 can be written as

$$G_c = \pi r^2 h G_{vc} + 2\pi r h \gamma_{ac} + 2\pi r^2 \gamma_{oc}^{\text{eff}}, \quad (4)$$

with G_{vc} as the Gibbs free energy per unit volume of the bulk crystalline phase. The Gibbs free energy of a cylindrical particle of the same size but in amorphous phase a is given by

$$G_a = \pi r^2 h G_{va} + 2\pi r^2 \gamma_{oa}^{\text{eff}}, \quad (5)$$

where G_{va} is the Gibbs free energy per unit volume of the amorphous bulk phase and

$$\gamma_{oa}^{\text{eff}} = \gamma_{oa} e^{-l/l_0} \quad (6)$$

is the effective specific interface energy, which describes [in analogy to Eqs. (2) and (3)] the influence of the interface o/a on the formation of the amorphous cylindrical particle. For $l=0$, i.e., $h=d$, the term (6) takes into account that the amorphous phase a has a true interface with the oxide phase o (Fig. 4). For $l \gg l_0$, or equivalently $l \rightarrow \infty$, the effective specific interface energy γ_{oa}^{eff} tends to zero, which corresponds to pure bulk behavior of the amorphous phase.

The nucleation energy barrier is given by the difference of the Gibbs free energies $\Delta G = G_c - G_a$. Using the above Eqs. (2)–(6) we find

$$\Delta G = -\pi r^2 h \Delta G_v + 2\pi r h \gamma_{ac} + 2\pi r^2 \Delta \gamma_{\text{eff}}, \quad (7)$$

where

$$\Delta G = G_{va} - G_{vc} > 0$$

and

$$\Delta \gamma_{\text{eff}} = \gamma_{ac} + (\gamma_{oc} - \gamma_{ac} - \gamma_{oa})e^{-l/l_0}. \quad (8)$$

The terms in Eq. (7) describe the change in bulk free energy, the energy necessary for forming the new a/c interface, and the influence of the boundaries formed by the oxide material o , respectively. l is given by $l = (d-h)/2$, with $d \geq h$ (cf. Fig. 4). Equation (7) represents a generalization of the nucleation model of Persans, Ruppert, and Abeles² and Honma *et al.*,¹¹ which can be rederived if $l=0$ or equivalently $h=d$ is chosen in Eq. (7):

$$\Delta G_{\text{Pers}} = -\pi r^2 d \Delta G_v + 2\pi r d \gamma_{ac} + 2\pi r^2 (\gamma_{oc} - \gamma_{oa}). \quad (9)$$

If $\gamma_{oc} - \gamma_{oa} > 0$ then crystal nucleation is inhibited, but $\gamma_{oc} - \gamma_{oa} < 0$ will enhance the formation of crystal nuclei as mentioned before in Refs. 2 and 11. However, in both Refs. 2 and 11 the height h of the nucleus is geometrically coupled with the interface by fixing $h=d$ from the very beginning, which leads to a wrong behavior of the maximum value of ΔG as a function of d .

In the presented model h and d are geometrically independent parameters which are coupled *energetically* by Eq. (8). This allows us to consider the Gibbs free energy change in Eq. (7) as a function of both the variables r and h .

The nucleation barrier is given by the maximum of ΔG [Eq. (7)], which is defined by

$$\frac{\partial \Delta G}{\partial r} = 0, \quad \frac{\partial \Delta G}{\partial h} = 0. \quad (10)$$

The calculations can easily be carried out. However, the presence of the exponential function in Eq. (8) leads to a nonlinear equation for r and h , which can only be solved numerically. Due to the fact that the specific interface energies are not well known and in order to keep the calculation as simple as possible, we make the following approximation: We ignore the fact that $\Delta \gamma_{\text{eff}}$ depends on the size h of the nucleus and replace l in Eq. (8) by an average value \bar{l} . Since l varies between the minimum value $l_{\text{min}}=0$ (for $h=d$) and the maximum value $l_{\text{max}}=d/2$ (for $h=0$) we choose as the average value $\bar{l}=(l_{\text{min}}+l_{\text{max}})/2=d/4$. There are other possible averaging procedures. With our approximation for l in Eq. (7) we derive from Eq. (10) for the critical radius of the nucleus

$$r^* = \frac{2\gamma_{ac}}{\Delta G_v}, \quad (11)$$

and for the critical cylinder height of the nucleus

$$h^* = \frac{4\Delta \gamma_{\text{eff}}}{\Delta G_v}. \quad (12)$$

Inserting Eqs. (11) and (12) into Eq. (7) yields for the nucleation barrier

$$\Delta G^* = \frac{8\pi\gamma_{ac}^2\Delta \gamma_{\text{eff}}}{\Delta G_v^2}, \quad (13)$$

where $\Delta \gamma_{\text{eff}}$ is given by the exponential function

$$\Delta \gamma_{\text{eff}} = \gamma_{ac} + (\gamma_{oc} - \gamma_{ac} - \gamma_{oa})e^{-d/4l_0}. \quad (14)$$

Assuming that the amorphous-to-crystalline transition is induced by a thermally activated process, the transition temperature T can be estimated from

$$kT \sim \Delta G^*, \quad (15)$$

where k is Boltzmann's constant. Equation (15) can be motivated as follows. The nucleation rate is essentially proportional to the Boltzmann factor, $N \sim N/t \sim \exp(-\Delta G^*/kT)$, which, in turn, means that the time t for the formation of a certain number N of nuclei is given by $t/N \sim \exp(\Delta G^*/kT)$. If

we define the crystallization temperature T_c , as usual, by the requirement that a certain fixed number N_c of nuclei is generated at a given fixed time t_c , the crystallization temperature follows as

$$\Delta G^*/kT_c = \ln(t_c/N_c) + \text{const.} \quad \text{or} \quad kT_c \sim \Delta G^*.$$

If we further define the bulk crystallization temperature T_{ac} by

$$kT_{ac} \sim \Delta G_{ac}^*, \quad (16)$$

where ΔG_{ac}^* is the bulk nucleation barrier that can be derived from Eqs. (13) and (14) in the limit $d \rightarrow \infty$,

$$\Delta G_{ac}^* = \frac{8\pi\gamma_{ac}^3}{\Delta G_v^2}, \quad (17)$$

we obtain $T_c/T_{ac} = \Delta G^*/\Delta G_{ac}^*$, or

$$T_c = T_{ac} \frac{\Delta \gamma_{\text{eff}}}{\gamma_{ac}} = T_{ac} \left(1 + \frac{\gamma_{oc} - \gamma_{ac} - \gamma_{oa}}{\gamma_{ac}} e^{-d/4l_0} \right). \quad (18)$$

This result has the functional form of the empirically found relationship Eq. (1). Through the comparison with Eq. (1) the following relations can be derived:

$$T_{\text{melt}} = T_{ac} \frac{\gamma_{oc} - \gamma_{oa}}{\gamma_{ac}}, \quad (19)$$

$$C = 4l_0. \quad (20)$$

From our data fitting the crystallization temperature T_c tends to the temperature of the melting point of bulk crystalline silicon $T_{\text{melt}} = 1683$ K in the limit of zero thickness of the Si layer, whereas in the limit of a thick layer we get $T_c(d \rightarrow \infty) \approx T_{ac} = 973$ K as we have mentioned before.¹⁵ We obtained similar results for germanium using the typical Ge values (see Table I) and taking into account the error of our measurements (± 25 K). According to our theoretical results represented in Eqs. (18) and (19), the enhancement of T_c in the limit $d \rightarrow 0$ is related to the difference in the specific interface energies of the interfaces between the crystalline and amorphous phases involved. However, if one takes into consideration that the melting of the crystalline phase is likewise associated with the nucleation of a crystalline-to-liquid interface, the above results at least give us a hint as to why there exists such a good empirical correlation between T_c for $d \rightarrow 0$ and the melting point T_{melt} of the crystalline phase. While this point requires further investigation, the relationships (18)–(20) are used in the following section to estimate a lower limit for the layer thickness below which no crystallization can occur.

DISCUSSION

The above crystallization model describes in detail the extraordinary crystallization behavior of ultrathin layers in a superlattice structure. As mentioned before, the screening length l_0 might be related to the range of interatomic forces or to the length of elastic interactions between the respective interfaces. In our experiments we found $C \approx 2.52$ – 2.56 nm independent of the material (Ge,Si). Hence, from Eq. (20)

the screening length is given by $l_0 \approx 0.64$ nm, which is closely related to the lattice parameter of Si and Ge and corresponds to the range of 2–3 interatomic distances.

Until the nucleus reaches a critical radius the embryo seed needs energy to grow. Therefore, in order to reduce the free energy, clusters with smaller size tend to shrink, while those with sizes larger than the critical size tend to grow. As can be seen in Eq. (13) the nucleation barrier scales strongly with the specific interface energies and the volume gain in free energy. In addition, using Eq. (12) the critical height of the nucleus depends exponentially on the thickness, leading to a larger critical height for thinner layers. Nucleus formation normally is not a rapid process. A number of atoms have to be accidentally in the right order to form a nucleus. The number of nuclei resulting from the thermal fluctuation of atoms is determined by the above-mentioned Boltzmann distribution. The probability for nucleus growth increases with increasing temperature. Changes in the interface free energy will significantly influence the formation of nuclei. For example, approximately 19 atoms are arranged across a thin layer of 5 nm using an average atomic distance a of 0.27 nm. Assuming a crystal with a critical radius of ~ 1 nm arranged in the middle of the 5 nm layer, only seven atomic layers separate the tiny nucleus from the SiO_2 interface. This will be even less for thinner Si layers capped with $a\text{-SiO}_2$ in a superlattice structure. Thus, the nuclei are strongly influenced by the additional surface tension of the Si/SiO₂ interface. This can be rationalized more precisely utilizing the crystallization model developed above.

From the experimental results in Table I and the theoretical prediction Eq. (19), the following numerical relationship between the yet unknown interface energies γ_{oc} and γ_{oa} can be deduced:

$$\gamma_{oc} - \gamma_{oa} = 1.73\gamma_{ac}. \quad (21)$$

With an amorphous/crystalline interface energy per atom of about $\sigma_{ac} = 0.105$ eV/atom,¹ and the average interatomic distance $a = 0.27$ nm in crystalline Si,¹ the value of γ_{ac} is estimated to be $\gamma_{ac} = \sigma_{ac}/a^2 = 1.440$ eV/nm² = 0.231 J/m². With this value for γ_{ac} Eq. (21) yields that γ_{oc} is about 2.491 eV/nm² (or 0.399 J/m²) larger than γ_{oa} . This result is reasonable in so far as the amorphous oxide to crystalline silicon ($a\text{-SiO}_2/c\text{-Si}$) interface o/c is expected to be energetically more unfavorable than the amorphous oxide to amorphous silicon ($a\text{-SiO}_2/a\text{-Si}$) interface o/a .

The minimum lateral size r^* of the cylindrical nucleus given by Eq. (11), which is determined only by γ_{ac} and the change in the bulk Gibbs free energy per unit volume ΔG_v , is in the present approximation the same as the radius of a free spherical crystalline nucleus in bulk amorphous silicon. With $\Delta G_v = \Delta g_v/a^3$, where $\Delta g_v = 0.100$ eV/atom is the free-energy change associated with the crystallization of one atom,¹ and $\gamma_{ac} = \sigma_{ac}/a^2$, we derive from Eq. (11)

$$r^* = \frac{2\sigma_{ca}}{\Delta g_v} a = 0.567 \text{ nm}. \quad (22)$$

For the free spherical nucleus this corresponds to a cluster of $i = 4\pi r_v^3/3a^3 \approx 39$ atoms,¹ while for the lateral size of our

cylindrical nucleus this corresponds to $i^* = 4\pi r_v^2/a^2 \approx 55$ atoms within a circular section perpendicular to the cylinder axis.

The minimum height h^* of the cylindrical nucleus, Eq. (12), depends via the effective specific interface energy Eq. (14) exponentially on the layer thickness. For large layer thickness, bulk behavior is restored, yielding $h^* = h_{\text{bulk}}^* = 4\gamma_{ac}/\Delta G_v = 2r^* = 1.134$ nm for $d \rightarrow \infty$, which corresponds to a fairly symmetrical nucleus with almost the same volume as a spherical nucleus with radius r^* . For very small layer thickness the condition $l \geq 0$ or equivalently $h^* \leq d$ must be fulfilled in our model (see Fig. 4), which gives a lower bound d_{min} for d . In order to determine d_{min} we write Eq. (12) for h^* in the form

$$h^* = 2r^* \left[1 + \left(\frac{\gamma_{oc} - \gamma_{oa}}{\gamma_{ac}} - 1 \right) e^{-d/4l_0} \right], \quad (23)$$

where we have utilized Eqs. (11) and (14). Further, using the numerical values available from Eqs. (21) and (22) and for l_0 , we find from the requirement $h^* = d$ for $d = d_{\text{min}}$ by a simple numerical procedure $d_{\text{min}}/4l_0 = 0.62$ or $d_{\text{min}} = 2.48l_0 \approx 1.59$ nm. Thus, we expect that for layer thickness $d < d_{\text{min}} \approx 1.6$ nm for the $a\text{-Si/SiO}_2$ system no crystallization can occur whatever the temperature. This is in fairly good agreement with our measurements on the Si/SiO₂ interface system, where crystallization has been observed in the case of stoichiometric SiO₂ interfaces up to $d \approx 1.9$ nm (see Fig. 2). The value of $d_{\text{min}} = 1.6$ nm is also larger than one would expect from purely geometrical considerations, i.e., by relating d simply to the size of the nucleus under bulk conditions $h^* = 2r^* = 1.1$ nm, which yields $d_{\text{min}} = 1.1$ nm. The higher value of d_{min} is clearly a consequence of a strong increase in the nucleation barrier caused by the continuous increase of the effective specific interface energy Eq. (14) when the a/c and o/c interfaces approach each other, which is unavoidable during nucleation at small d .

In addition, effects are expected for nonstoichiometry of the oxide ($\text{SiO}_x, x < 2$). In this case, annealing at high temperatures will result in bond relaxation and rearrangement in the nonstoichiometric oxide. Diffusion of the oxygen is expected, resulting in SiO₂ regions and Si-rich clusters. Such a process is used in bulk SiO_x films for the creation of randomly distributed Si nanocrystals in a SiO₂ matrix. Also, the inhomogeneous strain in the interface regions will be reduced if the interface is nonstoichiometric. Both effects, which are not included in our model, will reduce the crystallization temperature especially for superlattices with thin (below 3 nm) Si layers, in agreement with the experimental results (see Fig. 2). On the other hand, in the limit of thick layers, the crystallization results in bulk amorphous behavior. In this case the size of the critical nucleus is small compared to the layer thickness. Hence, the influence of the oxide interface and the inhomogeneous strain will be reduced. In addition, we expect for very thick layers a more spherical shape of the nucleus with still amorphous material around the crystals, and the evidence of growth faults for medium layer thickness (7–30 nm).

CONCLUSION

We have shown the exponential scaling of crystallization temperature with layer thickness for (Si, Ge)/SiO₂ superlattices. Using an empirical model this behavior can be reduced to basic material properties like the bulk amorphous crystallization temperature and the melting point. A crystallization model was presented that takes into account the different interface energies and materials. Using our model, an exponential increase of the crystallization temperature with decreasing layer thickness can be derived in agreement with the empirical model. This has been achieved by introducing the concept of an effective interface energy that interpolates between the true oxide/crystalline interface energy and the true

amorphous/crystalline interface energy by means of an order parameter varying continuously with interface spacing. The model yielded a lower bound for the layer thickness below which no crystallization can occur for the Si/SiO₂ system, which is in good quantitative agreement with our experimental observations.

ACKNOWLEDGMENTS

The authors are grateful to Dr. P. Veit and Dr. J. Bläsing for TEM and x-ray investigations. One of the authors (M.Z.) is grateful for financial support from the Volkswagen Stiftung.

*Present address: MPI für Mikrostrukturphysik, Weinberg 2, 06120 Halle, Germany. Email address: zacharias@mpi-halle.de

- ¹C. Spinella, S. Lombardo, and F. Priolo, *J. Appl. Phys.* **84**, 5383 (1998).
- ²P. D. Persans, A. Ruppert, and B. Abeles, *J. Non-Cryst. Solids* **102**, 130 (1988).
- ³G. V. M. Williams, A. Bittar, and H. J. Trodah, *J. Appl. Phys.* **67**, 1874 (1990).
- ⁴M. Zacharias, in *Advances in Solid State Physics*, edited by B. Kramer (Vieweg, Braunschweig, 1999), p. 131.
- ⁵J. Gonzalez-Hernandez and R. Tsu, *Appl. Phys. Lett.* **42**, 90 (1983).
- ⁶M. Zacharias, J. Bläsing, P. Veit, L. Tsybeskov, K. Hirschman, and P. M. Fauchet, *Appl. Phys. Lett.* **74**, 2614 (1999).
- ⁷Z. H. Lu, D. J. Lockwood, and J.-M. Baribeau, *Solid-State Electron.* **40**, 197 (1996).
- ⁸S. Miyazaki, Y. Ihara, and M. Hirose, *J. Non-Cryst. Solids* **97&98**, 887 (1987).
- ⁹J.-M. Baribeau, D. J. Lockwood, G. C. Aers, and M. W. C. Dharma-Wardana, in *Common Themes and Mechanisms of Epitaxial Growth*, edited by P. Fuoss, J. Tsao, D. W. Kisker, A. Zangwill, and T. F. Kuech, *MRS Symposia Proceedings No. 312* (Materials Research Society, Pittsburgh, 1993), p. 145.
- ¹⁰J. Bläsing, P. Kohlert, and M. Zacharias, *J. Appl. Crystallogr.* **31**, 589 (1998).
- ¹¹I. Honma, H. Hotta, K. Kawai, H. Komiyama, and K. Tanaka, *J. Non-Cryst. Solids* **97&98**, 947 (1987).
- ¹²J. F. Van der Veen, B. Pluis, and A. W. Denier van der Gon, in *Chemistry and Physics of Solid Surfaces*, Vol. 7, edited by R. Vanselow and R. Howe (Springer, Berlin, 1988), p. 455.
- ¹³M. Zacharias, J. Bläsing, P. Veit, L. Tsybeskov, K. Hirschman, and P. M. Fauchet, *J. Non-Cryst. Solids* **266-269**, 640 (2000).